



Triple-negative breast tumors are dependent on mutant p53 for growth and survival

Denada Dibra^a, Sydney M. Moyer^{a,b}, Adel K. El-Naggar^c, Yuan Qi^d , Xiaoping Su^d, and Guillermina Lozano^{a,b,1}

Contributed by Guillermina Lozano; received May 30, 2023; accepted July 21, 2023; reviewed by Tomoo Iwakuma and Maureen E. Murphy

The *TP53* tumor suppressor gene is mutated early in the majority of patients with triple-negative breast cancer (TNBC). The most frequent *TP53* alterations are missense mutations that contribute to tumor aggressiveness. We developed an autochthonous somatic K14-Cre driven TNBC mouse model with p53R172H and p53R245W mutations in which mutant p53 can be toggled on and off genetically while leaving the tumor microenvironment intact and wild-type for p53. These mice develop TNBCs with a median latency of 1 y. Deletion of mutant p53R172H or p53R245W in vivo in these tumors blunts their tumor growth and significantly extends survival of mice. Downstream analyses revealed that deletion of mutant *Trp53* activated the cyclic GMP–AMP Synthase–Stimulator of Interferon Genes pathway but did not cause apoptosis implicating other mechanisms of tumor regression. Furthermore, we determined that only tumors with stable mutant p53 are dependent on mutant p53 for growth.

mouse models | mutant p53 stability | tumor cell vulnerabilities | breast cancer

Tumor-initiating events can dictate tumor dependencies and vulnerabilities (1). In particular, the *TP53* tumor suppressor gene is deleted or mutated in 84% of triple-negative/basal-like breast cancers, and 75% of *HER2*-amplified breast cancers, which suggests that p53 loss is a driver of the disease (2). The most common *TP53* alterations are missense mutations that encode mutant proteins that lack transcriptional activity. Most missense mutations occur in the DNA-binding and tetramerization domains, where they attenuate the ability of p53 to bind DNA and regulate gene transcription (3). In addition, many p53 missense mutants have gain-of-function (GOF) activities that result in changes in cell shape, mobility, and invasiveness, ultimately leading to metastasis (4–8). The stability of mutant p53 proteins contributes to their GOF activities through interactions with other proteins (6, 7, 9–11).

The physiological role of mutant p53 in tumor maintenance is not well understood in vivo. Mouse models to study this relationship are complicated due to the presence of mutant p53 in all cells and the inability to distinguish the role of mutant p53 in cancer cells vs. the tumor microenvironment (TME). For example, the removal of mutant p53 in spontaneously arising lymphomas and colon adenocarcinomas in vivo reduced tumor growth (12, 13). While the mechanism by which lymphomas regressed is unknown, ablation of mutant p53 in colorectal cancers resulted in a Stat3-mediated inhibition of tumor growth and invasion (13). However, in these studies, mutant p53 is expressed in all cells, and deletion of mutant *Trp53* occurs in tumor cells as well as cells in the TME obfuscating the results. Using human breast cancer cell lines, Freed-Pastor et al. found that the depletion of mutant p53 is sufficient to phenotypically revert breast cancer organoids to a more benign and acinar structure, which suggests that mammary tumors are also addicted to mutant p53 (9). However, these studies were performed *in vitro* and thus in the absence of a microenvironment and immune system.

We recently developed somatic mouse models expressing mutant p53 using *Trp53* conditional alleles, which allow the TME to retain wild-type p53 (7, 14, 15). In the breast model, p53 missense mutations expressed only in the breast epithelium yielded metastatic triple-negative, Her2 enriched, and luminal B breast cancers that disseminated early (15). Thus, we were poised to examine the role of mutant p53 dependency in a somatic breast cancer model *in vivo*. In the present study, mutant p53R172H or p53R245W expression driven specifically by *K14-Cre* in epithelial cells, led to triple-negative breast cancer (TNBC) with a median latency of 1 y. The targeted deletion of mutant *Trp53* only in cancer cells bearing either p53 mutation caused tumor regression and extended survival of mice which was not due to apoptosis. Tumors that failed to stabilize mutant p53 were not dependent on mutant p53 for growth.

Significance

The physiological relevance of mutant p53 in tumor cell survival was studied in a mouse model where mutant p53 can be toggled on and off genetically leaving the tumor microenvironment intact and wild-type for p53. Two hot spot p53 mutations drive development of triple-negative breast cancer and deletion of either mutant blunts tumor growth, causes cell death independent of apoptosis, and significantly extends survival of mice revealing a potential vulnerability for future therapies.

Author affiliations: ^aDepartment of Genetics, The University of Texas MD Anderson Cancer Center, Houston, TX 77030; ^bGenetics and Epigenetics Program, The University of Texas MD Anderson Cancer Center UTHealth Graduate School of Biomedical Sciences, Houston, TX 77030; ^cDepartment of Pathology, The University of Texas MD Anderson Cancer Center, Houston, TX 77030; and ^dDepartment of Bioinformatics and Computational Biology, The University of Texas MD Anderson Cancer Center, Houston, TX 77030

Author contributions: D.D. and G.L. designed research; D.D. and S.M.M. performed research; D.D. contributed new reagents/analytic tools; D.D., S.M.M., A.K.E.-N., Y.Q., and X.S. analyzed data; and D.D., X.S., and G.L. wrote the paper.

Reviewers: T.I., University of Kansas Medical Center; and M.E.M., Wistar Institute.

Competing interest statement: G.L. is on the scientific advisory board for PMV, receives honoraria from various universities for her lectures, and owns stock in PMV.

Copyright © 2023 the Author(s). Published by PNAS. This article is distributed under Creative Commons Attribution-NonCommercial-NoDerivatives License 4.0 (CC BY-NC-ND).

¹To whom correspondence may be addressed. Email: gglozano@mdanderson.org.

This article contains supporting information online at <https://www.pnas.org/lookup/suppl/doi:10.1073/pnas.2308807120/-DCSupplemental>.

Published August 14, 2023.

Results

Mutant p53 R172H Drives Development of TNBCs. To study the role of mutant p53 in breast cancer, we used the somatic breast tumor model driven by a common hotspot mutation, p53R172H (p53R175H in humans). Mice heterozygous for the conditional *Trp53^{wm-R172H}* allele have functional wild-type p53 and are not prone to develop cancer (15). Cre-mediated recombination allows expression of *Trp53^{R172H}* in a cell- or tissue-specific manner (Fig. 1*A*). We developed a cohort of mice with *Trp53^{wm-R172Hfl}*, *K14-Cre*, and *Rosa26^{LSL} CAS9-P2A-EGFP/+* alleles (abbreviated P¹⁷²CC mice). Mutant *Trp53^{wm-R172H}* and floxed *Trp53^{fl}* alleles were used because approximately 80% of patients with *TP53* mutant breast tumors also lack wild-type *TP53*. *K14-Cre* is expressed in progenitor epithelial cells of the mammary, thyroid, and skin (16). *K14-Cre* thus allowed expression of only mutant p53R172H protein and Cas9 (from the *Rosa26^{LSL} CAS9-P2A-EGFP/+* locus) in epithelial cells, which were also labeled with green fluorescent protein (GFP). The surrounding TME retained wild-type p53 and did not express Cas9 or GFP. Control mice had *Trp53^{wm-R172Hfl}* and *Rosa26^{LSL} CAS9-P2A-EGFP/+* (P¹⁷²C mice) alleles. Approximately 35% of the background in this cohort is BALB/c since this background sensitizes mice to breast cancer development (15, 17).

Forty-seven P¹⁷²CC mice developed breast cancer with median survival of 376 d (Fig. 1*B*). Twelve mice developed a second cancer. Ten percent of mice developed head and neck or skin tumors and were excluded from the study. Ten control P¹⁷²C mice survived 500 to 800 d; none developed breast or skin tumors (Fig. 1*B*). Breast tumors varied in pathology: 47% of the breast tumors were adenocarcinomas, 31% were breast sarcomas followed by 22% sarcomatoid adenocarcinomas (Fig. 1 *C* and *D*). Quantification by real-time qPCR (RT-qPCR) of *Esr1*, *Pgr*, and *Erbb2* (representing ER, PR, and Her2) with appropriate positive (ovarian tissue or mammary tissue from MMTV-ErbB2 transgenic mice) and negative controls (spleen tissue) was used to determine the molecular subtypes (15). In the P¹⁷²CC cohort, 95% (56 of 59) of breast tumors were TNBCs and 5% (3 of 59) were *Pgr*-positive (Fig. 1*E*).

p53 missense mutants drive metastatic incidence (6, 8). Metastatic incidence of mammary tumors from P¹⁷²CC was low, 7.3% (3/41). Lungs for 6 of 47 animals were not available. These tumors metastasized to the lung. Metastases were observed in adenocarcinomas (13%, 2/15) and sarcomatoid adenocarcinomas, (9.1%, 1/11) but not in sarcomas (0 of 15) (Fig. 1 *F* and *G*). In sum, p53R172H as the initiating genetic abnormality drives TNBC formation with a median latency of 1 y.

Somatic TNBCs with p53R172H Depend on Mutant p53 for Maintenance. To delete mutant p53 in these TNBCs, we used CRISPR-Cas9. These breast tumors express Cas9 from the *Rosa26^{LSL} CAS9-P2A-EGFP/+* locus in tumor cells but not in the TME (Fig. 2*A*). Recombinant adeno-associated virus (AAV) is a preferred vector for introducing genetic material in vivo because AAV has a small, easy-to-manipulate genome (18). Furthermore, AAV efficiently delivers guide RNAs (gRNAs) and deletes target genes in vivo (19). We generated AAV8 (abbreviated AAV throughout) viral particles expressing two gRNAs in a single vector that target p53 exons 2 and 7, thus deleting the transactivation and DNA-binding domains. These two gRNAs for *Trp53* were validated individually in vivo, and each results in 44% indels (18, 20). AAV expressing the two gRNAs targeted mutant p53 efficiently and deleted mutant p53 in a murine breast cancer cell in as few as 72 h (Fig. 2*B*). Two nontargeting gRNAs were similarly cloned and used as controls.

To demonstrate the ability of AAV to effectively infect autochthonous tumors in vivo, we injected AAV particles expressing tdTomato (AAV8-EF1-tdTomato-WPRE-hGH) intratumorally. Only cells infected with AAV will express tdTomato. Injection of 5×10^9 virus particles into a tumor 0.8 cm in diameter resulted in tdTomato expression in 35% of tumor cells within 72 h (Fig. 2*C*). Larsson et al. showed that genetically reactivating wild-type p53 in 25% of mutant-p53 tumor cells demonstrates a dramatic therapeutic response, which suggests that 35% infection efficiency would be sufficient to observe biological effects (21). To increase the likelihood of infecting a larger percentage of cells, we performed three consecutive intratumoral injections on days 0, 3, and 8 (Fig. 2*D*). P¹⁷²CC mice were randomized to receive AAV expressing gRNAs for p53 (AAV-Δmut-p53) or AAV expressing nontargeting gRNAs (AAV-Control). Because these tumors have only one mutant *Trp53* allele (the other is a *Trp53^{fl}* allele that lost exons 1 to 10 with K14-Cre recombinase), AAV-Δmut-p53 deletes the mutant allele. Prior to treatment, both groups had similar tumor volumes (Fig. 2*E*).

As early as 3 d after the first injection, tumors injected with AAV-Δmut-p53 grew more slowly than those injected with AAV-Control, and 50% of the tumors injected with AAV-Δmut-p53 shrank within this time frame (Fig. 2*F*). Of 22 tumors (18 mice) injected with AAV-Δmut-p53, 20 (91%) showed a decreased growth rate. Conversely, all 9 tumors injected with AAV-Control grew rapidly, and mice bearing these tumors were humanely killed owing to tumor size (Fig. 2*G*). The median survival of all mice that received AAV-Δmut-p53 (28 d) was twice that of the mice that received AAV-Control (14 d), with one AAV-Δmut-p53 treated mouse surviving 100 d (Fig. 2*H*). The effect on survival upon mutant *Trp53* deletion is likely better, as six mice were humanely killed because they developed secondary breast tumors in independent fat pads (marked with an arrow, Fig. 2*I*). The criteria in killing mice were based on cumulative tumor burden. Two P¹⁷²CC mice had no response to AAV-Δmut-p53 (Fig. 2*F*, asterisk) and were humanely killed.

Next, we determined if dependence on mutant p53 was based on pathology of these mammary tumors. The two nonresponders were sarcomatoid adenocarcinomas and were not included in this analysis. In adenocarcinomas, deletion of mutant *Trp53* increased median survival from 16.5 to 32.5 d (Fig. 2 *I, Left*). One animal with an adenocarcinoma treated with AAV-Δmut-p53, responded well to mutant *Trp53* deletion, but had to be killed at 12 d due to development of two additional tumors (marked with an arrowhead). Similarly, deletion of mutant *Trp53* in sarcomas significantly increased median survival from 13 d to 27 d (Fig. 2 *I, Middle*). Last, in sarcomatoid adenocarcinomas, survival improved from 20.5 to 26.5 but was not significant (Fig. 2 *I, Right*). In this case also, one of the animals had to be killed 16 d post treatment due to occurrence of a secondary tumor even though the first tumor regressed (marked with an arrowhead). If this animal is excluded, the survival analysis is significantly different ($P = 0.03$). In sum, these genetic experiments definitively showed that the majority of murine P¹⁷²CC TNB tumors depended on mutant p53 for their survival.

Tumors Are Dependent on Stable Mutant p53 for Growth. Two P¹⁷²CC mice had no response to AAV-Δmut-p53 (Fig. 2*F*, asterisks) and were humanely killed. We hypothesized that tumors from these mice lacked stable mutant p53 protein. Therefore, immunofluorescence imaging was used to assess all tumors in the P¹⁷²CC cohort for mutant p53 protein levels (12, 22, 23). Among the mice that received AAV-Δmut-p53, the two tumors that were nonresponders had a similar growth rate as controls (Fig. 3*A*).

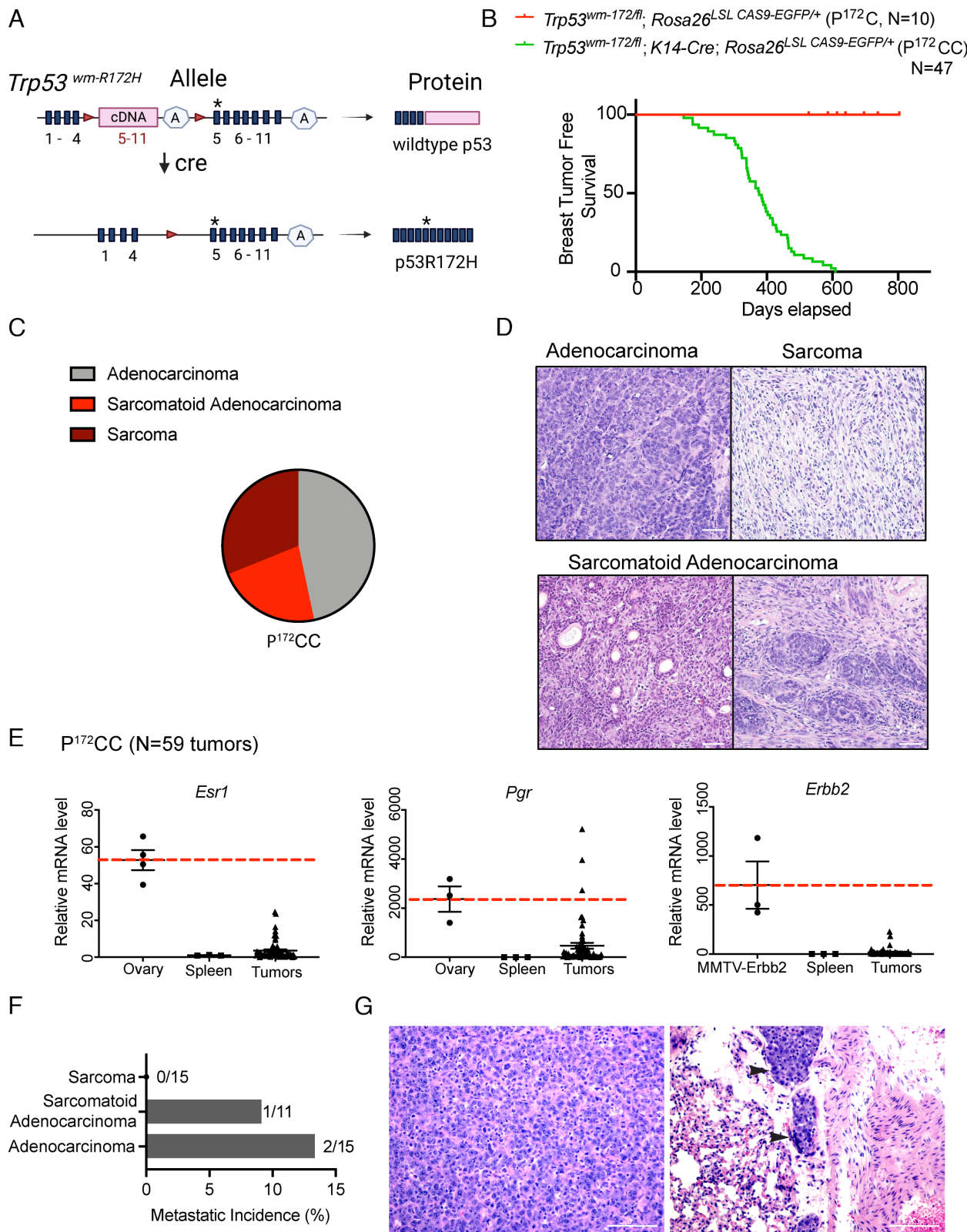


Fig. 1. Mutant p53 R172H drives development of TNBCs. (A) A schematic representation of the *Trp53*^{wm-R172H} allele, which normally expresses wild-type p53 (15). Cre recombinase removes the wild-type cDNA sequences and converts the allele to one expressing the p53R172H mutant. Red triangles indicate loxP sites; "A" indicates the *Trp53* native polyadenylation signal; asterisks indicate the CGC to CAC alteration at codon 172 in exon 5, which generates the p53R172H mutant (15). (B) Kaplan-Meier breast-specific survival curves for $P^{172}CC$ mice (N = 47), with mutant p53R172H expression specifically in epithelial cells; and control $P^{172}C$ mice lacking Cre (N = 10). (C) Pathological subtypes of mammary tumors from $P^{172}CC$ mice: adenocarcinoma, 47%; sarcoma, 31%; and sarcomatoid adenocarcinoma 22%. (D) Representative hematoxylin and eosin-stained sections of mammary tumors from mice with different pathological subtypes. (Scale bars, 50 μ m.) (E) RT-qPCR analysis for *Esr1*, *Pgr*, and *Erbb2* in 59 breast tumors from 47 $P^{172}CC$ mice. Mouse ovaries and spleens from normal mice, and breast tumors from MMTV-ErbB2 mice were used as positive and negative controls, respectively (15). Each dot represents one sample; the red dashed line represents median of positive controls. (F) Comparison of metastases incidence of mammary tumors from the $P^{172}CC$ cohort based on pathological subtypes. (G) Hematoxylin and Eosin-stained sections of a primary adenocarcinoma (Left) and metastatic lesions in the lung (Right). (Scale bars, 500 μ m.) Black arrowheads point to metastatic lesions in the lung.

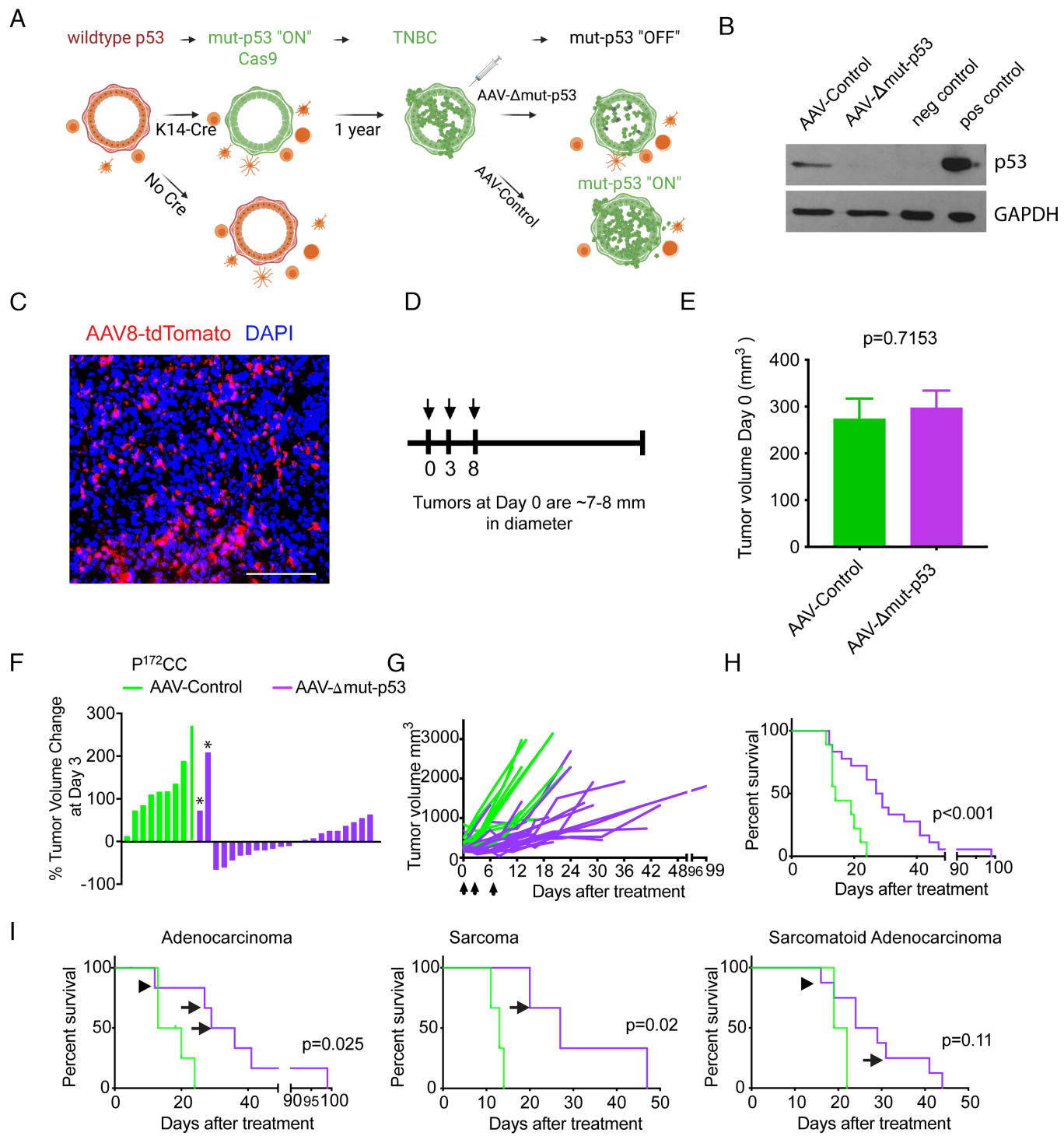


Fig. 2. Somatic TNBCs with p53R172H depend on mutant p53 for maintenance. (A) A schematic of the experimental process of turning on and off mutant p53. (B) A murine cell line with mutant p53 was infected with AAV-Control or AAV-Δmut-p53 (1×10^5 genome copies/cell), and p53 levels were measured by western blotting 72 h after infection. (C) Detection of tdTomato in a frozen section of a P¹⁷²CC breast tumor injected with AAV-EF1-tdTomato-WPRE-hGH (which induces the expression of tdTomato in infected cells), 72 h after infection. (Scale bar, 100 μm). (D) Treatment regimen; arrows indicate days of AAV injections. (E) Tumor volumes of breast tumors from P¹⁷²CC mice prior to treatment with AAV-Control or AAV-Δmut-p53. (F) Waterfall plot of percent changes in tumor volume in P¹⁷²CC mice 3 d after the first AAV injection. *nonresponders after treatment with AAV-Δmut-p53. (G) Breast tumor growth (adenocarcinomas, sarcomas, and adenocarcinoma with sarcomatoid features) in individual P¹⁷²CC mice after three injections with AAV-Control or AAV-Δmut-p53. Arrows denote injection times. (H) Kaplan-Meier survival curves of all P¹⁷²CC mice with breast cancer treated with AAV-Control ($n = 9$) or AAV-Δmut-p53 ($n = 18$; $P < 0.001$). (I) Kaplan-Meier survival curves of P¹⁷²CC mice separated by pathological subtypes. Arrows and arrowheads indicate mice killed due to second tumor formation. Data are mean \pm SEM. Significant differences between groups was evaluated by Student's *t* test. Survival curve comparisons were made using a log-rank Mantel-Cox test.

Furthermore, survival of these two nonresponders was also similar to controls (Fig. 3B). Mutant p53 was nondetectable in these two nonresponding tumors from the P¹⁷²CC cohort (Fig. 3C). These data indicate that tumors driven by a p53 missense mutation are dependent on its stability for growth.

Mutant p53 Dependency In Vivo Is not Due to Apoptosis. To elucidate the mechanism(s) underlying dependency to mutant p53, we subjected adenocarcinomas from P¹⁷²CC mice treated with either AAV-Control ($n = 3$) or AAV-Δmut-p53 ($n = 6$) to bulk RNA sequencing (RNA-seq). All AAV-treated tumors were

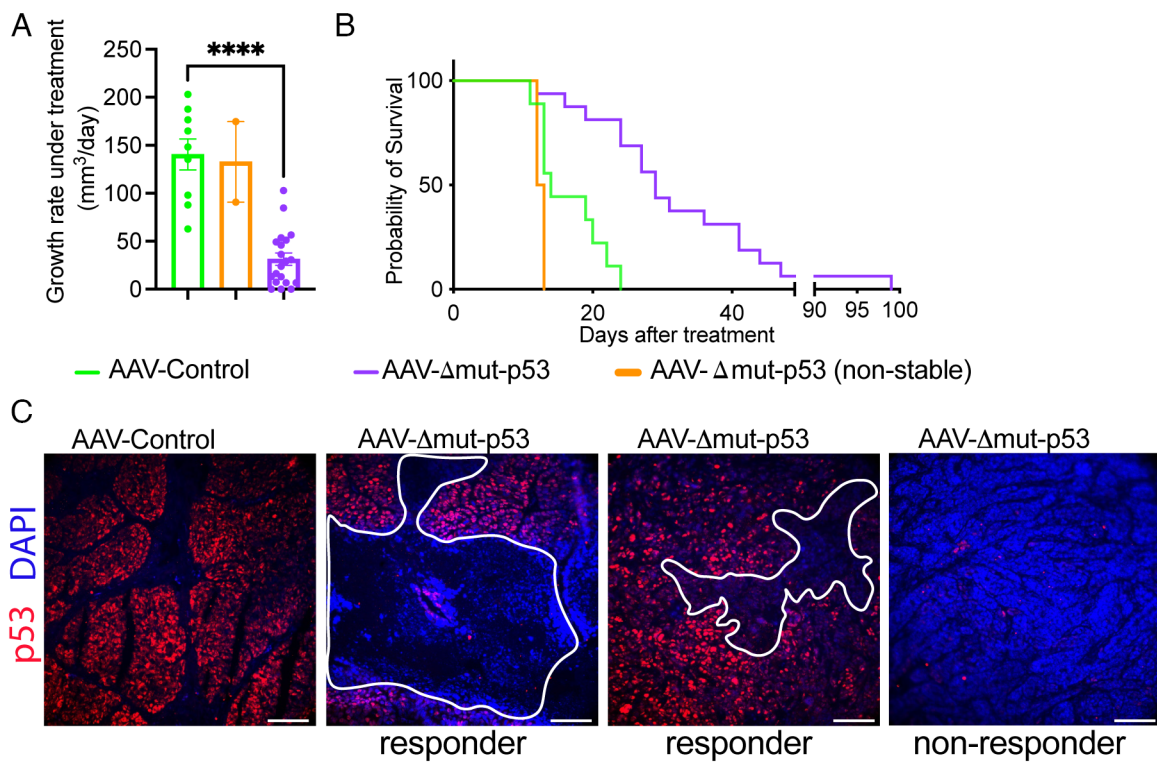


Fig. 3. Tumors are dependent on stable mutant p53 for growth. (A) Tumor growth rates for breast cancers treated with AAV-Control or AAV-Dmut-p53. (B) Kaplan-Meier survival curves of $P^{172}\text{CC}$ mice with breast cancer treated with AAV-Control ($N = 9$) or AAV-Dmut-p53 ($N = 18$; $P < 0.001$) with (16) or without (2) stable p53. (C) Immunofluorescence imaging of mutant p53 (red) and DAPI (blue) in breast tumors from four mice treated with AAV-Control or AAV-Dmut-p53. Outlined regions indicate tumor cell loss. (Scale bar, 100 μm .) **** $P < 0.0001$. Survival curve comparisons were made using a log-rank Mantel-Cox test.

harvested at end point; AAV-Dmut-p53 tumors showed evidence of cell loss as shown in Fig. 3C. In these adenocarcinomas, the top up-regulated pathways included NADH metabolic processes (Fig. 4A, Left). Furthermore, pathways involving immune-related pathways such as IFN α/β and IFN γ signaling, (Fig. 4A, Right), indicative of immune activation, were unregulated upon mutant *Trp53* deletion.

Post mutant *Trp53* deletion, we saw areas of tumor cell loss (Fig. 3C), which suggests that mutant p53 protected cells from some sort of cell death. Others have demonstrated in vitro that mutant p53 protects cells from apoptosis inducing agents (24). To determine whether mutant p53 protects cells from apoptotic cell death in vivo, we perused the RNA-seq data to determine whether apoptotic pathways were enriched upon mutant *Trp53* deletion. To our surprise, apoptotic pathways were not significantly enriched upon mutant *Trp53* deletion (Fig. 4B). Next, we determined if genes whose protein products induce apoptosis, namely *Bbc3* (*Puma*), *Bid*, *Bax*, and *Bcl2l11* (*Bim*) were differentially expressed in tumors with or without mutant *Trp53* deletion. No differences were observed in expression of these apoptotic targets (Fig. 4C). In sum, changes in metabolism and immune cell activation but not apoptosis drive mutant p53 dependency in these TNBC tumors.

Mutant p53R245W Drives Development of TNBCs that Depend on Mutant p53 for Maintenance In Vivo. To also determine if differences between mutant p53 proteins exist, we developed a similar cohort of mice driven by the p53R245W (p53R248W in humans) contact mutant. The $P^{245}\text{CC}$ cohort consisting of 23 mice with *Trp53*^{wm-R245W/+}, *K14-Cre*, and *Rosa26*^{LSL Cas9-P2A-EGFP/+} alleles expressed the p53R245W mutant, Cas9, and GFP only in epithelial cells (Fig. 5A). $P^{172}\text{CC}$ and $P^{245}\text{CC}$ mice developed breast cancer with median survival of 376 and 405

d, respectively; this difference was not statistically significant (Fig. 5B). Breast tumors varied in pathology: 65% of the breast tumors were adenocarcinomas, 30% breast sarcomas, and 5% sarcomatoid adenocarcinoma (Fig. 5C). Metastatic incidence of all mammary tumors from $P^{245}\text{CC}$ was low, 7.7% (1/13), comparable to the 7.3% observed in breast tumors of the $P^{172}\text{CC}$ cohort. Similar to $P^{172}\text{CC}$, adenocarcinomas but not sarcomas developed metastatic nodules in the lungs (12.5%, 1/8, Fig. 5D). Too few sarcomatoid adenocarcinomas (one) were seen in this model to estimate metastatic incidence. Real-time qPCR (RT-qPCR) with appropriate positive and negative controls was used to determine the molecular subtypes (15). In the $P^{245}\text{CC}$ cohort, all tumors except one were TNBCs (Fig. 5E). The outlier was *Esr1* positive.

Like those in the $P^{172}\text{CC}$ cohort, tumors in the $P^{245}\text{CC}$ cohort were dependent on mutant p53, as 62% of these tumors showed shrinkage 3 d after mutant *Trp53* deletion and 100% showed a reduced growth rate (Fig. 5F and G). Moreover, $P^{245}\text{CC}$ mice with mutant *Trp53* deletion lived significantly longer than controls (Fig. 5H). The number of tumors in this cohort were too small to separate by tumor subtypes. These genetic experiments definitively showed that murine $P^{172}\text{CC}$ and $P^{245}\text{CC}$ TNBC tumors were dependent on mutant p53 for their survival.

Next, we wanted to determine if apoptosis was the mechanism of cell death in tumors with deletion of the p53R245W mutation. We assayed for apoptosis shortly after deletion of mutant *Trp53* in $P^{245}\text{CC}$ tumors (3 d after second injection, tumors injected on days 0 and 3) of AAV-Control ($n = 5$) or AAV-Dmut-p53 ($n = 8$). At this time point, tumors grew slower after deletion of mutant *Trp53* than AAV-Control mice, averaging 50% of controls. Histological analyses performed for cleaved caspase 3 three d after second treatment (deletion of mutant *Trp53*) revealed a similar number of cells positive between control and mutant *Trp53* deleted

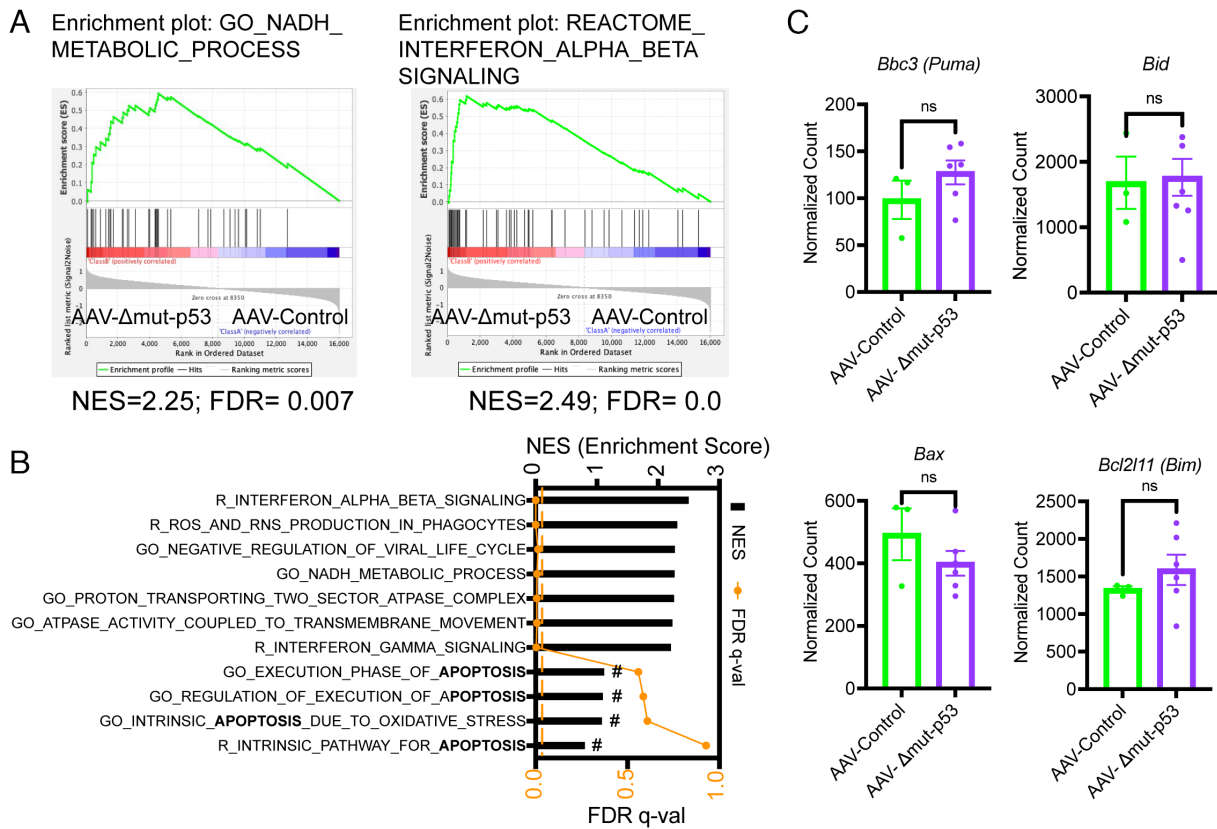


Fig. 4. Mutant p53 dependency in vivo is likely not due to apoptosis. (A) GSEA enrichment plots indicating that deletion of mutant *Trp53* in breast cancers from $P^{172}CC$ mice induces enrichment in gene sets associated with metabolism, and immune activation processes, including NADH metabolic processes and Interferon α/β . NES, normalized enrichment score; FDR, False discovery rate q-value. (B) GSEA pathways from datasets GO and Reactome, ranked by NES (black columns) and FDR (orange line) q-values from tumors treated with AAV-Control or AAV-Δmut-p53. Dotted orange line, FDR q-values significance set at <0.05 . #, apoptotic pathways are nonsignificant (FDR q-values ranging between 0.55 to 0.93 indicated by the orange line). (C) Normalized read counts from tumors treated with AAV-Control or AAV-Δmut-p53 for *Bbc3* (*Puma*), *Bid*, *Bax*, and *Bcl2l11* (*Bim*) genes whose protein products induce apoptosis from the RNA-seq dataset. Ns, not significant.

tumors (Fig. 5*I*), indicating that mutant p53 cell dependency in vivo does not involve apoptosis.

Activation of the cGAS-STING (cyclic GMP-AMP Synthase-Stimulator of Interferon Genes) Pathway Post Mutant *Trp53*

Deletion In Vivo. Given that pathways involving immune-related events such as IFN α/β and IFN γ signaling were enriched upon *Trp53* deletion (in the absence of apoptosis), we delved deeper into these pathways. GSEA revealed that gene sets associated with cytosolic sensing of pathogen-associated DNA and Rig I like receptor innate-like pathway signaling were enriched upon mutant *Trp53* deletion (Fig. 6*A*) indicative of the cGAS-STING pathway activation. This pathway has emerged as a critical mechanism in induction of innate immune defense programs and anti-cancer therapies (25). The activation of interferon regulatory factor 3 (IRF3) and its induction of type I interferons such as IFN α/β are the best-understood processes coordinated by cGAS-STING activation (25). Therefore, we determined if expression levels of IRF3 transcriptional targets change post mutant *Trp53* deletion. The levels of *Cxcl10* and *Ifit1* were significantly up-regulated in tumors in vivo post mutant *Trp53* deletion when compared to controls (Fig. 6*B*).

Phosphorylation of Sting at Ser366 allows the STING-TBK1 complex to recruit IRF3, enabling nuclear translocation and target gene induction, thereby serving as a pathway-specific read-out marker (26). Indeed, *Trp53* deletion in vivo elevated pSTING Ser366 positive tumors cells in breast tumors of $P^{172}CC$ and $P^{245}CC$ genotypes, indicative of cGAS-STING pathway activation

(Fig. 6*C*). In sum, our in vivo data demonstrate the mutant p53 inhibits activation of the cGAS-STING pathway.

Discussion

We developed two somatic models of mutant p53–driven breast cancer that retain a wild-type p53 stroma and immune system. Tumors were driven by initiating hotspot p53 missense mutations, p53R172H or p53R245W, corresponding to p53R175H and p53R248W in patients. Both mutations occur in the DNA binding domain and disrupt the ability of p53 to bind DNA, therefore, resulting in loss of function. Both proteins also have additional properties that increase tumor aggressiveness, invasion, metastasis, and drug resistance (4–11). Utilizing in vivo genetic tools, we found that TNBCs are dependent on mutant p53R172H and p53R245W for survival. In this model, mutant p53 is the initiating driving mutation. Of note, 42% of human TNBCs have p53 missense mutations suggestive of a driver mutation. In addition, evolutionary studies across various cancers from 2,583 patients suggest that *TP53* is an early clonal mutation (27). It is possible that deletion of mutant p53 has little impact depending on other oncogenic alterations or timing of p53 mutation. Additional in vivo studies are needed to address this possibility. Furthermore, this study uncovered that tumors are dependent on stable mutant p53 for growth. Such data support previous studies indicating that mutant p53 stability is a prerequisite for GOF phenotypes (12, 22, 23). For example, in an osteosarcoma model, mutant p53 stability was correlated with increased metastasis (28). These data indicate that

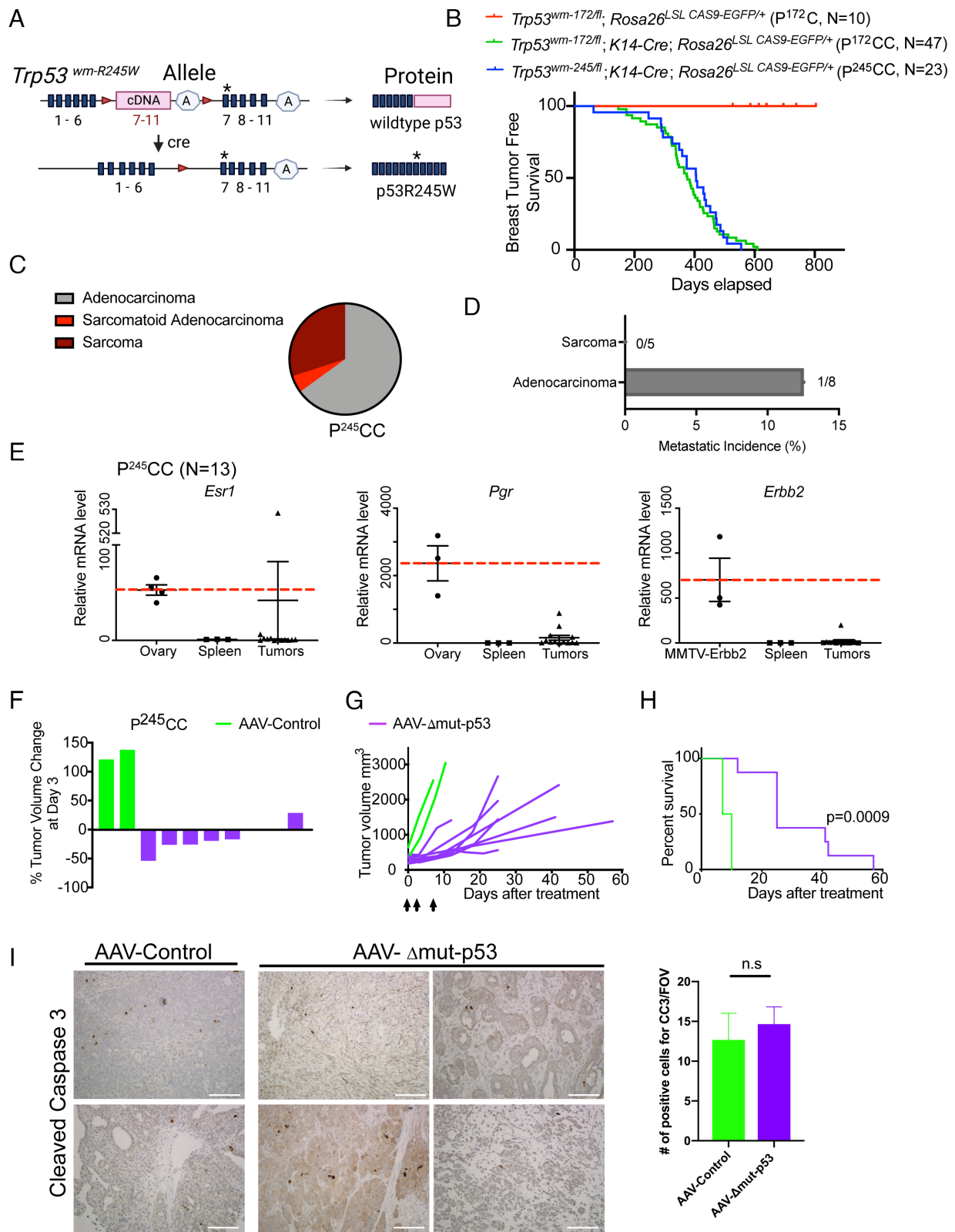


Fig. 5. Mutant p53R245W drives development of TNBCs that depend on mutant p53 for maintenance in vivo. (A) A schematic representation of the *Trp53^{wm-R245W}* allele, which normally expresses wild-type p53 (15). Cre recombinase removes the wild-type cDNA sequences and converts the allele to one expressing p53R245W mutant. Red triangles indicate loxP sites; “A” indicates the *Trp53* native polyadenylation signal; asterisks indicate the GCC to TGG mutations at codon 245 in exon 7, which generate the p53R245W mutant. (B) Kaplan-Meier breast-specific survival curves for *Trp53^{wm-172fl}, K14-Cre, Rosa26^{LSL CAS9-P2A-EGFP/+}* (*P*¹⁷²*C*) mice (*N*=47), and *Trp53^{wm-245fl}, K14-Cre, Rosa26^{LSL CAS9-P2A-EGFP/+}* (*P*²⁴⁵*CC*) mice (*N*=23), with mutant p53 expression specifically in epithelial cells; and control *Trp53^{wm-172fl}, Rosa26^{LSL CAS9-P2A-EGFP/+}* (*P*¹⁷²*C*) mice lacking Cre (*N*=10). (C) Pathological subtypes of mammary tumors from *P*²⁴⁵*CC* mice: adenocarcinomas 65%, sarcomas 30%, sarcomatoid adenocarcinomas 5%. (D) Comparison of metastasis incidence of mammary tumors based on pathological subtypes. (E) RT-qPCR analysis for *Esr1*, *Pgr*, and *Erbb2* in breast tumors from *P*²⁴⁵*CC* mice. Mouse ovaries and spleens from normal mice, and breast tumors from MMTV-ErbB2 mice were used as positive and negative controls, respectively (15). Each dot represents one sample; the red dashed line represents median of positive controls. (F) Waterfall plot of percent changes in tumor volume in *P*²⁴⁵*CC* mice 3 d after the first AAV injection. (G) Breast tumor growth of individual *P*²⁴⁵*CC* mice after injections with AAV-Control or AAV-Δmut-p53. (H) Kaplan-Meier survival curves of *P*²⁴⁵*CC* mice with breast cancer treated with AAV-Control (*N*=2) or AAV-Δmut-p53 (*N*=8; *P*<0.0009). (I) Immunohistochemical staining for cleaved caspase 3 (CC3) in tumors from *P*²⁴⁵*CC* injected with AAV-Control (*n*=5) or AAV-Δmut-p53 (*n*=8) 6 d after two injections. [Scale bars, 500 μm (Left).] CC3 staining was quantified in three fields of view (FOV) per sample (Right).

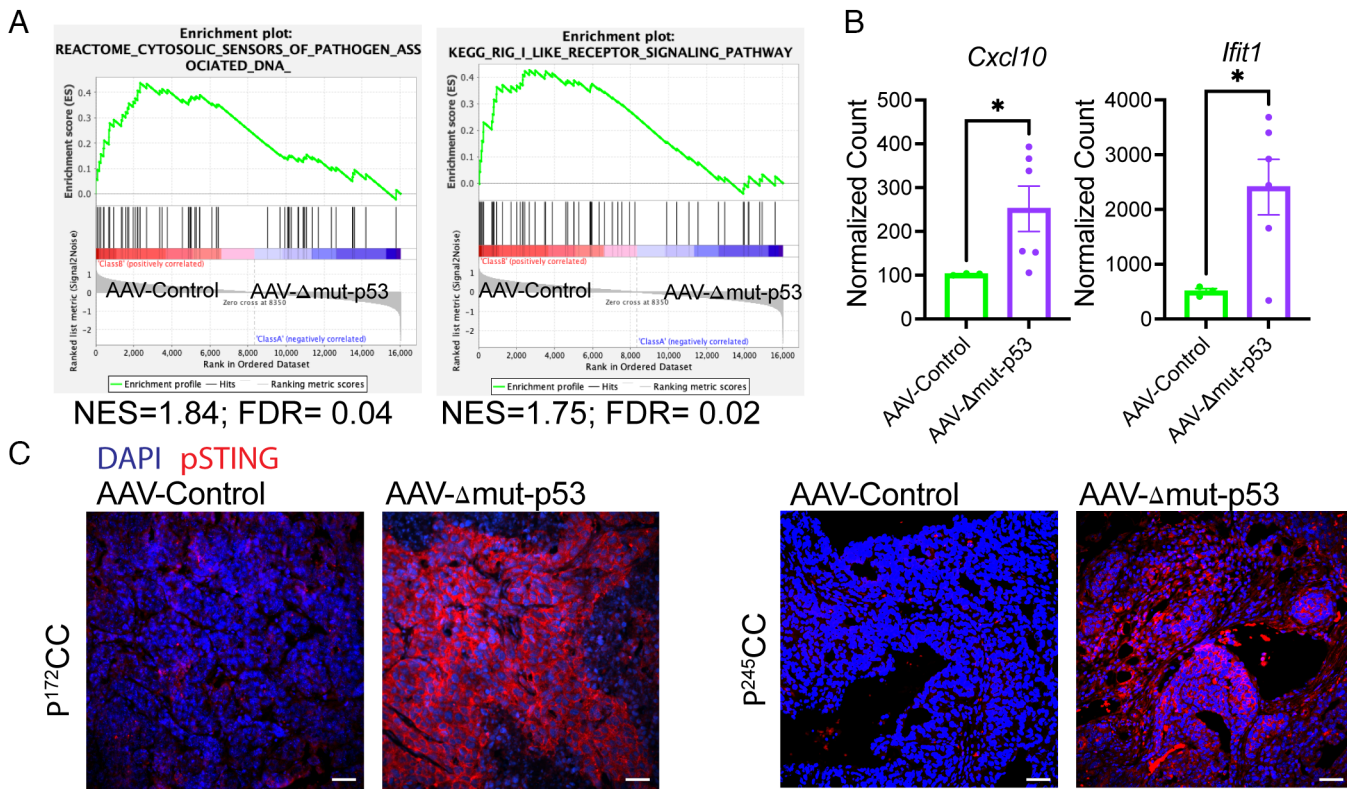


Fig. 6. Activation of the cGAS-STING pathway post mutant *Trp53* deletion in vivo. (A) GSEA enrichment plots indicating that deletion of mutant *Trp53* in breast cancers from P¹⁷²CC mice induces enrichment in gene sets associated cytosolic sensing of pathogen associated DNA and Rig I like receptor signaling. NES, normalized enrichment score; FDR, False discovery rate q-value. (B) Normalized read counts from tumors treated with AAV-Control ($N = 3$) or AAV-Δmut-p53 ($N = 6$) for *Cxcl10* and *Ifit1*. (C) Representative immunofluorescence imaging of pSTING-Ser366 (red) and DAPI (blue) of breast P¹⁷²CC (Left) or P²⁴⁵CC (Right) tumors treated with AAV-Control or AAV-Δmut-p53. (Scale bars, 50 μ m.)

mutant p53 proteins may be therapeutic targets in TNBCs. It further indicates the need to assay mutant p53 stability.

In our model, RNA-seq analyses revealed that deletion of mutant *Trp53R172H* only in tumor cells enriched for pathways involved in metabolism and immune-related pathways such as IFN α/β , and IFN γ and innate inflammatory response pathways, implicating tumor cell intrinsic and noncell intrinsic mechanisms of tumor regression. Data to support mutant p53 effects on the TME were described by Cook and Martinez; deletion of mutant p53 induces immune activation via the cGAS-STING pathway (29). We show in vivo that deletion of mutant p53 increases pSTING in these tumors. Additionally, although others have demonstrated in vitro that mutant p53 protects cells from apoptosis (24), we found that mutant p53 dependency in vivo does not occur through apoptosis. Multiple lines of evidence support this statement: first, we did not observe any significantly enriched apoptotic pathways upon mutant *Trp53R172H* deletion using RNA-seq even though tumor cell loss was observed at this time point; second, genes whose protein products induce apoptosis were not differentially expressed in tumors upon *Trp53R172H* deletion when compared to controls; third, when we assayed for apoptosis shortly after deletion of *Trp53* R245W in vivo (3 d after second AAV injection), no differences were observed in the number of apoptotic cells between control and mutant *Trp53* deleted tumors. On the other hand, even though we analyzed an early time point post mutant *Trp53* deletion to assay for apoptosis, we may have missed seeing dead cells.

Breast tumors in our K14-Cre driven mouse model are pathologically diverse encompassing adenocarcinomas, sarcomas, and a mixture of the two, sarcomatoid adenocarcinomas. Through lineage tracing, Keymeulen and colleagues found that all mammary

epithelial lineages derive from embryonic K14-expressing progenitors indicating Cre expression in multiple cell types (16). In a different Ad-Cre model with mutant p53R245W induced by injection of Ad-Cre directly into 10 to 12-wk-old mammary epithelium, pathologically diverse breast tumors were also observed including adenocarcinomas, spindle cell, and sarcomatoid adenocarcinomas (15). Therefore, in both the Ad-Cre and K14-Cre models, we observed pathologically diverse tumors suggesting that loss of glandular features, dedifferentiation, and cellular plasticity contribute to tumor diversity.

In numerous examples now, the potencies of these two p53 hotspot mutants differ based on cancer types, and presence of the second p53 wild-type allele. In our K14-Cre model, both p53R172H and p53R245W mutations with loss of the second *Trp53* allele drive TNBCs with a similar median survival of 1 y and similar metastatic incidence. However, in the Ad-Cre somatic breast tumor model, differences exist between *Trp53R172H* and *Trp53R245W* alleles in the presence of the wild-type allele (15). Only upon loss of the wild-type allele or treatment with low dose radiation (which causes loss of wild-type *Trp53*), is p53R172H able to induce breast tumorigenesis. Meanwhile, heterozygosity of *Trp53R245W* alone induces breast tumorigenesis. Furthermore, mammary tumors with a p53R245W mutation in the Ad-Cre model are more metastatic than those with p53R172H (15). Differences in timing of induction of p53 mutation, number of cells targeted, and time to tumor development allowing for metastatic tumors to grow may account for differences between the somatic Ad-Cre and K14-Cre models (15). In a somatic osteosarcoma model, Chachad et al. observed no differences in survival and metastatic incidence in osteosarcomas with either p53R172H or p53R245W mutations, in cohorts where the second *Trp53*

allele was either present or absent. Particularly intriguing from this study was that although potencies between the two mutants were similar, the mechanisms driving gain of function were different between the two mutants, with mutant p53R245W, but not the p53R172H interacting with Klf15 to drive a migration phenotype in somatic osteosarcomas (28). In sum, by generating an elegant mouse model to toggle on and off mutant p53 *in vivo*, we found physiological dependency on mutant p53R172H or p53R245W in these TNBCs, paving the way to uncover vulnerabilities in breast cancer patients with missense mutant p53.

Material and Methods

Mice. Previously characterized *Trp53*^{flox/flox} (30), *Trp53*^{wm-R172H}, *Trp53*^{wm-R245W} (15), *K14-cre* (01XF1, NCI Repository), and *Rosa26*^{LSL CAS9-P2A-EGFP/+} (024857, Jackson Laboratories) (18) mice were bred and crossed to generate P¹⁷²CC and P²⁴⁵CC mice. All mice were bred and maintained in a mixed background (FVB, C57BL/6, BALB/c), and only female mice with mammary tumors were examined in the study. All mice were monitored daily. Animals with signs of physical distress or with large breast tumor volumes were killed. Tumor diameter was measured with calipers. At end point after killing the mouse, we noticed that some of these spontaneous breast tumors invaginate internally (not visible), and true measurement was possible only after mice were killed upon dissection. Tumor volume was estimated using the formula ($\text{length} \times \text{width}^2$) $\times \pi/8$. All animal studies and procedures were approved by MD Anderson's Institutional Animal Care and Use Committee. Genotyping was carried out as described previously (15). See *SI Appendix, Table S1* for primer sequences. The rate of tumor growth was calculated using the formula $(V_{\text{euth}} - V_0)/(T_{\text{euth}} - T_0)$, where V_{euth} and T_{euth} are the tumor volume and treatment days, respectively, at the time the mice were killed; V_0 is the tumor volume at the start of treatment; and $T_0 = 0$.

AAV Treatment. Once primary breast tumors reached approximately 0.7 to 0.8 cm in diameter, AAV8 virus particles (5×10^9 genome copies) suspended in 50 μL of sterile phosphate-buffered saline were injected intratumorally. Tumors were injected with AAV on days 0, 3, and 8.

Cloning and Virus Production. Two gRNAs targeting p53 that had been validated *in vivo* were used in this study (18, 20). Briefly, gRNA1 was inserted into an AAV plasmid (PX552; deposited by Dr. Feng Zhang in Addgene). The same was done for gRNA2. Subsequently, PCR amplification of the U6 promoter-driven gRNA 2 was subcloned into the vector containing gRNA1 so that each AAV plasmid had two gRNAs. Two nontargeting gRNAs were similarly cloned and used as controls. See *SI Appendix, Table S1* for sequences of the guides. Plasmids were confirmed by Sanger sequencing. High-titer and pure AAV8 viruses were generated by the Gene Vector Core at Baylor College of Medicine. Virus was titered using real-time qPCR. Each tumor was injected with 5×10^9 total genome copies. High-titer AAV8-EF1-tdTomato-WPRE-hGH (AAV-tdTomato; 2.6×10^{13} genome copies/ml) was purchased from the Gene Vector Core.

Histopathology and Immunohistochemistry. Tissues harvested from mice were fixed in 10% neutral buffered formalin saline and embedded in paraffin. Tissues were processed, embedded in paraffin, cut into 5- μm sections, and subjected to H&E staining in MD Anderson's Department of Veterinary Medicine and Surgery's histology laboratory. Immunohistochemistry was performed using standard methods with citrate buffer for 30 min of antigen retrieval (15). Slides were stained with antibodies against cleaved caspase-3 (#9664; Cell Signaling). Visualization was performed using biotinylated secondary antibody

kits (VECTASTAIN ABC and DAB kits, Vector Laboratories), with hematoxylin as the counterstain.

Immunofluorescence. Paraffin-embedded tumor sections were deparaffinized and rehydrated, and antigen retrieval was performed in tris(hydroxymethyl) aminomethane-thylenediaminetetraacetic acid (TRIS-EDTA) pH 9.0. Slides were blocked in PBS containing 3% fish gelatin (VWR) for 20 min. Tissue sections were incubated with an anti-p53 antibody (CM5, Leica Biosystems; 1:200) or pSTING S366 (Cell Signaling; 1:100) overnight at 4 °C and then incubated with a secondary antibody labeled with AlexaFluor 555 (Thermo Fisher Scientific; 1:600). The sections were counterstained with DAPI (Thermo Fisher Scientific). Images were acquired using a Nikon 80i upright widefield fluorescence microscope with NIS-Elements imaging software (Nikon).

RNA Extraction. Flash-frozen tissue was pulverized, and total RNA was prepared using TRIzol Reagent (Invitrogen) and purified using the RNeasy mini kit (Qiagen). Briefly, the homogenized tissues were incubated with 500 μL of Trizol at room temperature for 5 min. Chloroform was then added to the tissue/Trizol mixture (chloroform:Trizol, 1:5 in volume) and mixed by vortex mixing. The chloroform/tissue/Trizol mixture was incubated at room temperature for 3 min and then centrifuged at 12,000 $\times g$ for 30 min at 4 °C. The upper phase was transferred to a new tube; 1.5 volumes of 100% ethanol were added to the upper phase, and this combination was mixed thoroughly by inverting the tube several times and then loaded into the RNeasy spin column (Qiagen) as per the manufacturer's protocol.

RNA-seq. RNA extraction was performed as described above. RNA-seq was performed at MD Anderson's Advanced Technology Genomics Core with a HiSeq 4000 system, generating 76-bp paired-end reads. The sample library was prepared using the Illumina TruSeq stranded total RNA protocol. RNA-seq FASTQ files were processed through FastQC, a quality control tool used to evaluate the quality of sequencing reads at both the base and read levels. Samples that passed quality control were used in subsequent analyses. STAR alignment to a mouse reference genome (GRCm38) was performed with default parameters to generate RNA-seq BAM files (31). Aligned reads were summarized at the gene level using the STAR aligner. Gene-level annotation was carried out using the GENCODE annotation, which was downloaded from the GENCODE project (32). The raw count data were processed and normalized by DESeq2 software to identify differentially expressed genes (DEGs) between the two groups (33). The final *P*-value was adjusted using the Benjamini–Hochberg method. A gene expression cutoff (\log_2 fold change of ≥ 1.0 or ≤ -1.0 and an False discovery rate *q*-value of ≤ 0.05) was applied to select the most significant DEGs. Differential gene expression was further analyzed with several pathway enrichment tools, such as GSEA (34).

Statistical Analysis. All data are presented as mean \pm SEM. GraphPad Prism 9.0 was used to perform all statistical analyses. Statistical significance was evaluated with the Student's *t* test. *P* < 0.05 was considered significant. A log-rank Mantel–Cox test was used to compare Kaplan–Meier survival curves.

Data, Materials, and Software Availability. RNA-seq data have been deposited in Gene Expression Omnibus (GEO), with accession number GSE213822 (35). All study data are included in the article and/or *SI Appendix*.

ACKNOWLEDGMENTS. High-titer AAV-8 virus was generated at the Gene Vector Core at Baylor College of Medicine. All figure schematics were created with BioRender. We thank all members of the Lozano laboratory for helpful discussions, and Dr. Amanda Wasylisen for critical review of the manuscript. This research was supported by grants from the NIH grant CA82577 (G.L.), and Stand Up To Cancer grant SU2C-AACR-PS-25 (D.D.)

1. H. Ying *et al.*, Oncogenic Kras maintains pancreatic tumors through regulation of anabolic glucose metabolism. *Cell* **149**, 656–670 (2012).
2. D. C. Koboldt *et al.*, Comprehensive molecular portraits of human breast tumours. *Nature* **490**, 61–70 (2012).
3. W.A. Freed-Pastor, C. Prives, Mutant p53: One name, many proteins. *Genes Dev.* **26**, 1268–1286 (2012).
4. L. Aschauer, P.A. Muller, Novel targets and interaction partners of mutant p53 Gain-Of-Function. *Biochem. Soc. Trans.* **44**, 460–466 (2016).
5. M. P. Kim, G. Lozano, Mutant p53 partners in crime. *Cell Death Differ.* **25**, 161–168 (2018).
6. G. A. Lang *et al.*, Gain of function of a p53 hot spot mutation in a mouse model of Li-Fraumeni syndrome. *Cell* **119**, 861–872 (2004).
7. M. P. Kim *et al.*, Oncogenic KRAS recruits an expansive transcriptional network through mutant p53 to drive pancreatic cancer metastasis. *Cancer Discov.* **11**, 2094–2111 (2021).
8. K. P. Olive *et al.*, Mutant p53 gain of function in two mouse models of Li-Fraumeni syndrome. *Cell* **119**, 847–860 (2004).
9. W.A. Freed-Pastor *et al.*, Mutant p53 disrupts mammary tissue architecture via the mevalonate pathway. *Cell* **148**, 244–258 (2012).

10. S. B. Xiong *et al.*, Pla2g16 phospholipase mediates gain-of-function activities of mutant p53. *Proc. Natl. Acad. Sci. U.S.A.* **111**, 11145–11150 (2014).
11. M. Adorno *et al.*, A mutant-p53/smad complex opposes p63 to empower TGF beta-induced metastasis. *Cell* **137**, 87–98 (2009).
12. E. M. Alexandrova *et al.*, Improving survival by exploiting tumour dependence on stabilized mutant p53 for treatment. *Nature* **523**, 352–356 (2015).
13. R. Schulz-Heddergott *et al.*, Therapeutic ablation of gain-of-function mutant p53 in colorectal cancer inhibits Stat3-Mediated tumor growth and invasion. *Cancer Cell* **34**, 298–314.e7 (2018).
14. R. Pourebrahim *et al.*, Integrative genome analysis of somatic p53 mutant osteosarcomas identifies Ets2-dependent regulation of small nucleolar RNAs by mutant p53 protein. *Gene Dev.* **31**, 1847–1857 (2017).
15. Y. Zhang *et al.*, Somatic Trp53 mutations differentially drive breast cancer and evolution of metastases. *Nat. Commun.* **9**, 3953 (2018).
16. A. Van Keymeulen *et al.*, Distinct stem cells contribute to mammary gland development and maintenance. *Nature* **479**, 189–193 (2011).
17. J. G. Koch *et al.*, Mammary tumor modifiers in BALB/cJ mice heterozygous for p53. *Mamm. Genome* **18**, 300–309 (2007).
18. R. J. Platt *et al.*, CRISPR-Cas9 knockin mice for genome editing and cancer modeling. *Cell* **159**, 440–455 (2014).
19. F. A. Ran *et al.*, In vivo genome editing using *Staphylococcus aureus* Cas9. *Nature* **520**, 186–191 (2015).
20. W. Xue *et al.*, CRISPR-mediated direct mutation of cancer genes in the mouse liver. *Nature* **514**, 380–384 (2014).
21. C. A. Larsson *et al.*, Synergistic and additive effect of retinoic acid in circumventing resistance to p53 restoration. *Proc. Natl. Acad. Sci. U.S.A.* **115**, 2198–2203 (2018).
22. E. M. Alexandrova *et al.*, p53 loss-of-heterozygosity is a necessary prerequisite for mutant p53 stabilization and gain-of-function *in vivo*. *Cell Death Dis.* **8**, e2661 (2017).
23. T. Terzian *et al.*, The inherent instability of mutant p53 is alleviated by Mdm2 or p16INK4a loss. *Genes Dev.* **22**, 1337–1344 (2008).
24. B. S. Tan *et al.*, Mutant p53-R273H mediates cancer cell survival and anoikis resistance through AKT-dependent suppression of BCL2-modifying factor (BMF). *Cell Death Dis.* **6**, e1826 (2015).
25. A. Decout, J. D. Katz, S. Venkatraman, A. Ablasser, The cGAS-STING pathway as a therapeutic target in inflammatory diseases. *Nat. Rev. Immunol.* **21**, 548–569 (2021).
26. S. Liu *et al.*, Phosphorylation of innate immune adaptor proteins MAVS, STING, and TRIF induces IRF3 activation. *Science* **347**, aaa2630 (2015).
27. M. Gerstung *et al.*, The evolutionary history of 2,658 cancers. *Nature* **578**, 122–128 (2020).
28. D. Chachad *et al.*, Unique transcriptional profiles underlie osteosarcomagenesis driven by different p53 mutants. *Cancer Res.* **83**, 2297–2311 (2023), 10.1158/0008-5472.CAN-22-3464.
29. T. Cooks *et al.*, Mutant p53 cancers reprogram macrophages to tumor supporting macrophages via exosomal miR-1246. *Nat. Commun.* **9**, 771 (2018).
30. S. Marino, M. Vooijs, H. van Der Gulden, J. Jonkers, A. Berns, Induction of medulloblastomas in p53-null mutant mice by somatic inactivation of Rb in the external granular layer cells of the cerebellum. *Genes Dev.* **14**, 994–1004 (2000).
31. A. Dobin *et al.*, STAR: Ultrafast universal RNA-seq aligner. *Bioinformatics* **29**, 15–21 (2013).
32. J. Harrow *et al.*, GENCODE: The reference human genome annotation for The ENCODE Project. *Genome Res.* **22**, 1760–1774 (2012).
33. M. I. Love, W. Huber, S. Anders, Moderated estimation of fold change and dispersion for RNA-seq data with DESeq2. *Genome Biol.* **15**, 550 (2014).
34. A. Subramanian *et al.*, Gene set enrichment analysis: A knowledge-based approach for interpreting genome-wide expression profiles. *Proc. Natl. Acad. Sci. U.S.A.* **102**, 15545–15550 (2005).
35. D. Dibra *et al.*, Triple-negative breast tumors are dependent on mutant p53 for growth and survival. *Gene Expression Omnibus*. <https://www.ncbi.nlm.nih.gov/geo/query/acc.cgi?acc=GSE213822>. Deposited 20 September 2022.